www.elsevier.com/locate/csr

Numerical study on the summer upwelling system in the northern continental shelf of the South China sea

Zhi-you Jing, Yi-quan Qi, Zu-lin Hua, Hong Zhang

PII: S0278-4343(08)00366-X
DOI: doi:10.1016/j.csr.2008.11.008
Reference: CSR 1906

To appear in: *Continental Shelf Research*

Received date: 26 October 2007
Revised date: 1 July 2008
Accepted date: 26 November 2008

Cite this article as: Zhi-you Jing, Yi-quan Qi, Zu-lin Hua and Hong Zhang, Numerical study on the summer upwelling system in the northern continental shelf of the South China sea, *Continental Shelf Research* (2008), doi:10.1016/j.csr.2008.11.008

Numerical Study on the Summer Upwelling System in the Northern Continental Shelf of the South China Sea

Zhi-you JING[a,b,*], Yi-quan QI[b], Zu-lin HUA[a] and Hong ZHANG[c]

a. *State Key Laboratory of Hydrology-Water Resources and Hydraulic Engineering; College of Environmental Science and Engineering, key Laboratory of Integrated Regulation and Resource Development on shallow Lake of Ministry of Education, Hohai University, Nanjing 210098, China;*

b. *Key Laboratory of Tropical Marine Environmental Dynamics, South China Sea Institute of Oceanology, Chinese Academy of Sciences, Guangzhou 510301, China;*

c. *Griffith School of Engineering, Griffith University, Gold Coast, 9726 Australia.*

Abstract: A three-dimensional baroclinic nonlinear numerical model is employed to investigate the summer upwelling in the northern continental shelf of the South China Sea (NCSCS) and the mechanisms of the local winds inducing the coastal upwelling, associated with the QuikSCAT wind data. First, the persistent signals of the summer upwelling are illustrated by the climatological AVHRR (the Advanced Very High Resolution Radiometer) SST (Sea Surface Temperature) image over 1985-2006 and field observations in 2006 summer. Then, after the successful simulation of the summer upwelling in the NCSCS, four numerical experiments are conducted to explore the different effects of local winds, including the wind stress and wind stress curl, on the coastal upwelling in two typical strong summer upwelling regions of the NCSCS. The modeled results indicate that the summer upwelling is a seasonal common phenomenon during June-September in the NCSCS with the spatial extent of a basin-scale. Typical continental shelf upwelling characteristics are clearly shown in the coastal surface and subsurface water, such as low temperature, high salinity and high potential density in the east of the Hainan Island, the east of the

Leizhou Peninsula and the southeast of the Zhanjiang Bay (noted as the Qiongdong - QD), and the inshore areas from the Shantou Coast to the Nanri Islands of the Fujian Coast (noted as the Yuedong - YD). The analysis of the QuikSCAT wind data and modeled upwelling index suggests that the local winds play significant roles in causing the coastal upwelling, but the alongshore wind stress and wind stress curl have different contributions to the upwelling in the Qiongdong (QDU) and the coastal upwelling in the Yuedong (YDU), respectively. Furthermore, model results from the numerical experiments show that in the YD the stable alongshore wind stress is a very important dynamic factor to induce the coastal upwelling but the wind stress curl has little contribution and even unfavorable to the YDU. However, in the QD the coastal upwelling is strongly linked to the local wind stress curl. It is also found that not only the offshore Ekman transport driven by the alongshore wind stress, the wind stress curl-induced Ekman pumping also plays a crucial effect on the QDU. Generally, the wind stress curl even has more contributions to the QDU than the alongshore wind stress.

Key words: Upwelling; Numerical Study; Northern South China Sea; QuikSCAT Winds; AVHRR SST

1. Introduction

The South China Sea (SCS) is a large semi-enclosed tropical marginal sea in the northwest Pacific Ocean with a total area of 3.5 million km^2 and an average depth of over 2000 m (Figure 1(a)). It is connected with the East China Sea in the northeast through the Taiwan Strait, the Pacific Ocean and the Sulu Sea in the east, and the Java Sea and the Indian Ocean in the southwest. Its main feature is a broad continental shelf with depth shallower than 200 m and isobath parallel to the continental coastline (Su, 2004). The climate in the SCS is dominated by the East Asian monsoon system (Wyrtki, 1961; Su, 2004). In winter the northeast monsoon prevails in the SCS, whereas in summer the winds reverse their directions to the southwest. From spring to summer, the SST (Sea Surface Temperature) in some regions of the northern continental shelf of the South China Sea (NCSCS) does not monotonically increase with solar radiation, but continuously decreases after the onset of the southwest monsoon, resulting in persistent low temperature in summer (Li, 1993).

Upwelling is one of the most important processes in marine system, which plays an important role in the nutrient transport of the ocean and has significant impacts on fishery. Strong upwellings are usually linked to important fisheries throughout the world, such as the Peru upwelling and Benguela upwelling (Pauly and Christensen, 1995; Risien, et al., 2004). In the NCSCS the summer upwelling is one of the most outstanding features, which was first noticed in Hongkong Coast by Wyrtki (1961) and in the east of the Hainan Island and south of the Shantou Coast by Niino & Emery (1961). Later, Guan and Chen (1964) systematically investigated the NCSCS upwellings based on the First Nationwide Survey of China Seas during 1959-1960, and their research indicated that the summer southwest monsoon is the dominant dynamic factor to drive the coastal upwellings. In following years, intensive studies have been carried out to understand the local upwelling in the

inshore areas from the Shantou Coast to the Nanri Islands (noted as the Yuedong Upwelling - YDU) and the upwelling in the east of Hainan Island, the east of the Leizhou Peninsula and the southeast of the Zhanjiang Bay (noted as the Qiongdong Upwelling - QDU) using various field observations. (Zeng, 1986; Yu, 1987; Han & Ma, 1988; and Han et al. 1990). Li (1990, 1993) and Hong & Li (1991) had a further analysis of a 20 years historical water temperature, salinity and dissolved oxygen data in the NCSCS. Their results suggested that the summer upwelling is a seasonal common phenomenon with the spatial extent of a basin-scale in the NCSCS, which has been confirmed in the recent numerical simulation (Jing et al., 2007).

In the northeast of the NCSCS, the Taiwan Strait Upwelling (TSU) is regarded as an important part of the NCSCS upwelling system. It has attracted a lot of attention since it was reported by Chen et al. (1982) based on the observations in the 1970s. TSU were continuously studied in the 1980s (Xiao, 1988; Cai and Lennon, 1988; Li and Li, 1989). Subsequently, several other local upwellings in the Taiwan Strait were identified from hydrological, chemical, biological and satellite observations (Hong et al., 1991; Li., 1993; Hu et al., 2001; Tang et al., 2002; Shang et al., 2004; Tang et al., 2004). Based on the six cruises data during 1987-1988, Hong et al. (1991) systematically investigated the TSU and the response of ecosystem, as well as their potential dynamics mechanisms. Recently, the satellite observations such as AVHRR (the Advanced Very High Resolution Radiometer) SST and SeaWiFS Chlorophyll, are comprehensively exploited in ocean and coastal research. Hu et al. (2001) analyzed the AVHRR SST during 1996-1999 and compared with the survey data during 1997-1999, and found the new evidences of four local upwelling regions in the Taiwan Strait. The TSU and its variabilities in various time-scales have been studied intensively, including the short-term variability (Tang et al. 2002, Shang et al., 2004)

and the long-term variability (Tang et al., 2004). However, the QDU (as in Figure 2), another important part of the NCSCS upwelling system, has been studied and understood limitedly. Therefore, an improved understanding of the upwelling system in the NCSCS, especially about the QDU, is of great importance for both coastal environmental management and fish production.

The dynamics mechanism of the NCSCS upwelling is complicated. The upwelling is induced by many factors including the winds, bottom topography, shelf circulation, eddies and islands and capes. The alongshore wind stress has been identified as one of the most important dynamical factors to induce the NCSCS coastal upwelling (Cai et al., 1988; Hong and Li, 1991; Yan et al., 1997; Guo et al., 1998, Hu et al., 2003; Wu and Li, 2003). Another important factor, the local wind stress curl on the coastal upwelling was hardly understood in the NCSCS. In present study, the dynamics of the summer upwelling system in the NCSCS is investigated using the multiple satellite remote sensing observational data, survey data and the numerical model ECOMSED, a three-dimensional nonlinear baroclinic coast-ocean model. Realistic bottom bathymetry and sea surface heat flux are adopted in the model. The high spatial and temporal resolution QuikSCAT scatterometer wind data are firstly used in a dynamical study of the NCSCS upwelling. The QuikSCAT scatterometer wind data have been successfully applied to the study of the southern Benguela upwelling system (Blanke et al., 2005).

The aims of this paper are to: (1) analyze the distribution of the summer upwellings in the NCSCS based on the climatological AVHRR SST image over 1985-2006 (Figure 2) and the cruise observational data during 2006 summer (Figure 3); (2) numerically simulate the upwelling system by using a three-dimensional baroclinic nonlinear numerical model; (3) investigate the mechanisms of local winds inducing the coastal upwelling in the Qiongdong (QD) and the Yuedong (YD),

including the wind stress and wind stress curl.

This paper is organized as follows. Firstly, the persistent signals of upwelling in the NCSCS are presented by combining climatological remote sensing SST image and historical cruise observations, providing the essential backgrounds and evidences of summer upwellings in the NCSCS. Secondly, after the numerical model and main simulation parameters are introduced, the modeled results about the summer upwellings are analyzed. It includes the typical upwelling physical characteristics and the seasonal evolutions of the upwellings in two typical strong upwelling regions QD and YD. And then, associated with the QuikSCAT wind data and numerical experiments, the relationships and potential dynamic mechanism between the upwelling and local winds are discussed in details. Some conclusions can be found at the end.

2. Evidences of Summer Upwelling

Generally, when upwelling event occurs, the colder, higher salinity and nutrient-richer water will rise from the deep layers to replace the surface water. Therefore the appearance of the abnormal low temperature and high salinity in the surface and subsurface water are good indicators of the upwelling (Hu et al., 2001). Figure 2 shows the climatological summer SST distribution in the NCSCS, which is derived from JPL (Jet Propulsion Laboratory, NASA) data. Low temperature in the surface water can be detected clearly in both YD and QD, as shown in Figure 2. At YD, the low temperature regions are mainly located in the east of the Guangdong Coast and southwest of the Fujian Coast, as well as the Taiwan Shoal near the west of the Penghu Archipelagoes. The strong upwellings mostly lie in the inshore areas from Hongkong to the Nanri Islands. Particularly, in the Shantou and Xiamen Coast, the large and strong upwellings occur within 150~200 km from

the coast with the SST of about 2~3℃ lower than the offshore water. In addition, a “crescent shape” low temperature band is located in the Taiwan shoal near the west of the Penghu Archipelagoes, where the SST is 2~3℃ lower than that of the offshore water.

QDU is another important upwelling in the NCSCS. Figure 2 shows that the low temperature regions are mostly situated in the east and northeast of the Hainan Island, the east of Leizhou Peninsula and the southeast of the Zhanjiang Bay. It is noted that the strong upwelling regions are located along the coast from the south of Sanya to the west of Qizhou Archipelagoes, where the SST is generally 1~2℃ lower than the offshore water. During 19 July- 06 August 2006, the ‘908’ Special Marine Survey was conducted in the east of Hainan Island. The survey profiles are shown in Figure 3. The survey observational data were analyzed for a better understand the QDU. Figure 4 shows the horizontal distribution of the water temperature and salinity at different depths. It can be seen that the low temperature and high salinity water clearly exists in the inshore subsurface water along the coast from the Lingshui Bay to the Qizhou Archipelagoes including the eastern Leizhou Peninsula. The coastal low temperature band at 10m-depth is at least 5℃ lower and the salinity is about 0.3 psu higher than the offshore water. Figure 5 illustrates the vertical distributions of the water temperature and salinity along different cross-shelf sections. Both isotherm and isohaline over the shelf are uplifted towards the shore, and the cold water in the depth of 80-100 m is also uplifted to the inshore surface or subsurface by the coastal upwelling. D03 section (Figure 3) is from the east of Leizhou Peninsula, through the Qizhou Archipelagoes, to the continental slope of eastern Hainan Island. D03 section results (Figure 5) shows that the strong upwelling mainly occurs in the depth shallower than 100 m. The 22℃ isotherm along this section is uplifted to the depth of 50 m from the depth of 70 m approximately 250 km offshore to the depth of 20 m within 50 km of the coast.

Its averaged vertical temperature gradient (AVTG) is about 2.5×10^{-4}. In the D06 and D09 sections (Figure 5), the strong upwellings mostly occur at the depth less than 100 m within 130 km off the coast, and at 100 m depth within 100 km off the coast. Their AVTG are 4.0×10^{-4} and 4.2×10^{-4} respectively.

3. Numerical Model

3.1 Coast-Ocean Model

The model ECOMSED applied in present study is originated from the ECOM (Estuarine, Coastal and Ocean Model) based on the Princeton Ocean Model (POM) by Blumberg and Mellor (1996). It has been developed to a stable and reliable three-dimensional baroclinic nonlinear hydrodynamic model, especially for the coastal ocean and estuarine situation.

The primitive ocean equations are used to describe the velocity fields, the surface elevation, and the temperature and salinity fields for the ocean circulation. The hydrostatic assumption assumes the weight of the fluid identically balances the pressure; and the Boussinesq approximation assumes the difference in inertia is negligible but gravity is sufficiently strong to make the specific weight appreciably different between the two fluids. The basic governing equations are as follows.

Continuity Equation:

$$h_1 h_2 \frac{\partial \eta}{\partial t} + \frac{\partial}{\partial \xi_1}(h_2 u D) + \frac{\partial}{\partial \xi_2}(h_1 v D) + h_1 h_2 \frac{\partial \omega}{\partial \sigma} = 0; \quad (1)$$

Momentum Equations:

$$\frac{\partial(h_1h_2Du)}{\partial t}+\frac{\partial}{\partial\xi_1}\left(h_2Du^2\right)+\frac{\partial}{\partial\xi_2}\left(h_1Duv\right)+h_1h_2\frac{\partial(\omega u)}{\partial\sigma}$$
$$+Dv\left(-v\frac{\partial h_2}{\partial\xi_1}+u\frac{\partial h_1}{\partial\xi_2}-h_1h_2f\right)=-gDh_2\left(\frac{\partial\eta}{\partial\xi_1}+\frac{\partial H}{\partial\xi_1}\right) \quad (2)$$
$$-\frac{gD^2h_2}{\rho_0}\int_\sigma^0\left(\frac{\partial\rho}{\partial\xi_1}-\frac{\sigma}{D}\frac{\partial D}{\partial\xi_1}\frac{\partial\rho}{\partial\sigma}\right)d\sigma-D\frac{h_2}{\rho_0}\frac{\partial P_a}{\partial\xi_1}+\frac{\partial}{\partial\xi_1}\left(2A_M\frac{h_2}{h_1}D\frac{\partial u}{\partial\xi_1}\right)$$
$$+\frac{\partial}{\partial\xi_2}\left(A_M\frac{h_1}{h_2}D\frac{\partial u}{\partial\xi_2}\right)+\frac{\partial}{\partial\xi_2}\left(A_MD\frac{\partial v}{\partial\xi_1}\right)+\frac{h_1h_2}{D}\frac{\partial}{\partial\sigma}\left(K_M\frac{\partial u}{\partial\sigma}\right),$$

$$\frac{\partial(h_1h_2Dv)}{\partial t}+\frac{\partial}{\partial\xi_1}\left(h_2Duv\right)+\frac{\partial}{\partial\xi_2}\left(h_1Dv^2\right)+h_1h_2\frac{\partial(\omega v)}{\partial\sigma}$$
$$+Du\left(-u\frac{\partial h_1}{\partial\xi_2}+v\frac{\partial h_2}{\partial\xi_1}+h_1h_2f\right)=-gDh_1\left(\frac{\partial\eta}{\partial\xi_2}+\frac{\partial H}{\partial\xi_2}\right) \quad (3)$$
$$-\frac{gD^2h_1}{\rho_0}\int_\sigma^0\left(\frac{\partial\rho}{\partial\xi_2}-\frac{\sigma}{D}\frac{\partial D}{\partial\xi_2}\frac{\partial\rho}{\partial\sigma}\right)d\sigma-D\frac{h_1}{\rho_0}\frac{\partial P_a}{\partial\xi_2}+\frac{\partial}{\partial\xi_2}\left(2A_M\frac{h_1}{h_2}D\frac{\partial v}{\partial\xi_2}\right)$$
$$+\frac{\partial}{\partial\xi_1}\left(A_M\frac{h_2}{h_1}D\frac{\partial v}{\partial\xi_1}\right)+\frac{\partial}{\partial\xi_1}\left(A_MD\frac{\partial u}{\partial\xi_2}\right)+\frac{h_1h_2}{D}\frac{\partial}{\partial\sigma}\left(K_M\frac{\partial v}{\partial\sigma}\right);$$

Transport Equations of Temperature and Salinity:

$$h_1h_2\frac{\partial(D\theta)}{\partial t}+\frac{\partial(h_2u\theta D)}{\partial\xi_1}+\frac{\partial(h_1v\theta D)}{\partial\xi_2}+h_1h_2\frac{\partial(\omega\theta)}{\partial\sigma} \quad (4)$$
$$=\frac{\partial}{\partial\xi_1}\left(\frac{h_2}{h_1}A_HD\frac{\partial\theta}{\partial\xi_1}\right)+\frac{\partial}{\partial\xi_2}\left(\frac{h_1}{h_2}A_HD\frac{\partial\theta}{\partial\xi_2}\right)+\frac{h_1h_2}{D}\frac{\partial}{\partial\sigma}\left(K_H\frac{\partial\theta}{\partial\sigma}\right),$$

$$h_1h_2\frac{\partial(SD)}{\partial t}+\frac{\partial(h_2uSD)}{\partial\xi_1}+\frac{\partial(h_1vSD)}{\partial\xi_2}+h_1h_2\frac{\partial(\omega S)}{\partial\sigma} \quad (5)$$
$$=\frac{\partial}{\partial\xi_1}\left(\frac{h_2}{h_1}A_HD\frac{\partial S}{\partial\xi_1}\right)+\frac{\partial}{\partial\xi_2}\left(\frac{h_1}{h_2}A_HD\frac{\partial S}{\partial\xi_2}\right)+\frac{h_1h_2}{D}\frac{\partial}{\partial\sigma}\left(K_H\frac{\partial S}{\partial\sigma}\right);$$

State Equation:

$$\rho_{total}=\rho_{total}(\theta,S) \quad (6)$$

In the model, the horizontal orthogonal curvilinear coordinate and σ-coordinate, $\xi=\xi(x,y)$, $\eta=\eta(x,y)$, $\sigma=(z-\zeta)/(H+\zeta)$, are used, where η is the water surface elevation and H is the distance from the datum plane to the bottom. Thus σ ranges from σ=0 (for z=η) to σ= -1 (for z=-H). In the above equations (2-6), *u* and *v* are the velocity components in the ξ_1 and ξ_2 direction respectively; θ is potential temperature, S is salinity; f is the Coriolis parameter; g is the gravitational acceleration. The vertical mixing coefficients K_M and K_H are obtained from the second order turbulence closure scheme (Mellor and Yamada., 1982). Similarly, the horizontal mixing coefficients A_M and A_H for both momentum and heat/salinity are parameterized by the SMAGORINSKY's scheme

(Smagorinsky, 1963). ρ_0 and ρ respectively represent the reference density and the disturbance density in situ which meet the relation of $\rho_{total} = \rho + \rho_0$.

3.2 Model Configuration

The simulation domain in this study covers the whole SCS (99°00′E - 124°00′E, 0°00′N-25°00′N) (as shown in Figure 1 (a)). The model has a horizontal resolution of 10′×10′, and 25 sigma levels in the vertical direction. In this model, comprehensive physical processes, including wind forcing, heat flux and open boundary forcing, are taken into consideration. At the surface, the daily climatological QuikSCAT winds, averaged from 7-year's real-time daily QuikSCAT winds over 2000-2006, are adopted in this simulation. The wind data's spatial resolution is 0.25°×0.25°. The net heat flux of ocean surface is derived from SOC (Southampton Oceanography Centre) flux dataset (Josey, 2001). The initial temperature and salinity are obtained from the WOA01 (World Ocean Atlas 2001) (Boyer et al., 2002). As shown in Figure 1 (a), four lateral boundaries A-D are specified at the Karimata Strait, the east of Luzon Island, the east of Taiwan Island, and the Taiwan Strait, respectively. The radiation condition is used for the lateral boundaries. The monthly mean throughflows through the four lateral boundaries can be found in Table 1 based on the observations and previous research results (Fang et al., 1991).

Considering the slow process of the thermohaline adjustment, the model is integrated for 6 years in all. Firstly, the model is spinned up diagnostically for 12 months from the static condition, driven by climatological January winds, temperature, salinity and boundaries' throughflows. Then, the diagnostical outputs of January are stored as the initial fields for the further prognostical integration. After 5 years' spin-up, the prognostical modeled results show that the total integral

kinetic energy begins to change periodically, which suggests the integration has been in a numerically quasi-steady state. In this study, the monthly mean results of the 5th year are used for analysis of the upwelling in the NCSCS.

3.3 Numerical Experiment Schemes

As discussed in section 1, the alongshore wind stress is a very important dynamical factor to induce the NCSCS coastal upwelling in summer. But the effect of local wind stress curl is poorly understood. In order to obtain a better understanding on the effects of the wind stress and wind stress curl to the NCSCS upwelling, four numerical experiments as shown in Table 2 are designed to examine the effects of wind stress and wind stress curl on the coastal upwelling. We take the simulation run of the model as the control test. In Case A, the surface winds is removed to eliminate the wind influences; in Case B, the wind stress curl is excluded from the model and only the alongshore wind stress is set up with spatially uniform wind speed of 8.0 m/s, while other physical processes are kept unchanged; in Case C, the climatological QuikSCAT wind stress and wind stress curl are adopted; in Case D, the doubled wind stress and wind stress curl of QuikSCAT winds are used.

The upwelling-induced vertical potential density gradient (VPDG) is taken as an index to quantify the effects of the wind stress and wind stress curl on the NCSCS upwelling. The three typical sections of strong upwelling regions (as shown in Figure 1 (b)) are located in the south of Fujian Coast (Section I), near the Qinglan Bay (Section II) and the shelf break adjacent to the southern Lingshui Bay (Section III). Upon comparing the indexes in Sections I-III in all cases, the effects of the wind stress and wind stress curl on the coastal upwelling can be evaluated effectively.

4. Modeled Results

The model has been run as described above. Figure 6 illustrates the general summer circulation patterns at the depth of 5m layer, including the essential characteristics of main currents in the SCS. Low temperature and high salinity in the surface and subsurface waters are the typical physical characteristics in upwelling centres. The closed isolines around low temperatures or high salinities and the coastline can be used to identify the position of upwelling centre (Li, 1993). Figure 7 (a)-(d) show the modeled temperature, salinity, potential density in the subsurface water, where the upwelling physical characteristics can be identified clearly.

4.1 Modeled Continental Shelf Upwelling Characteristics

In Figure 7 (a)-(d), the typical continental shelf upwelling characteristics are clearly shown in the coastal surface and subsurface water. Two strong upwelling regions exist in the NCSCS. One of them is located in the east of Hainan Island, the east of Leizhou Peninsula and the southeast of Zhanjiang Bay, and the other one is at the inshore areas from the Shantou Coast to the Nanri Islands of Fujian Coast, which is coincided with what the AVHRR SST image shows. But the “crescent shape” low temperature band in the Taiwan shoal observed by satellite is not reproduced in the simulation. It is because that the model’s spatial resolution is not enough high, and the west of the Luzon Strait, including the Taiwan shoal, is dominated by the modeled Kuroshio current loop and the closed anticyclone eddy completely.

The modeled centres of the QDU are located at (111°10′E, 19°45′N) between the Qinglan Bay and the Qizhou Archipelagoes, and (110°15′E, 18°25′N) near the Lingshui Bay. The modeled

centres of the YDU are mainly located at (116°45′E, 22°50′N) and (118°E, 23°40′N) near the Shantou Coast and the Taiwan Shoal. The 5m-depth water temperature in the QDU (as shown in Figure 7 (a)) is about 28℃, 1.5℃ lower than the offshore water at the same latitude. The 15m-depth temperature is 24℃, 3.5℃ lower than offshore water and the salinity is 34 psu, 0.2 psu higher than offshore water. In the YDU (as shown in Figure 7), the upwelling centre temperature at 5m depth is about 28℃, 1.2~1.5℃ lower than that of the offshore at same latitude, and at 15m depth the temperature is 25℃, 3~3.5℃ lower than offshore water and the salinity is obviously higher than the offshore water.

4.2 Seasonal Evolution of upwelling

It is known that the physical and chemical water properties can be significantly changed in the upwelling season. The "two-peak distribution" is one of the most typical effects in the time series of the seasonal variation (Li, 1990). The time series of the modeled temperature in the 5m layer, averaged in the QD and YD upwelling regions, can be found as red curves in Figure 8 (a) and (b) respectively. The two temperature curves represent remarkable "two-peak distribution" characteristics. In the QD upwelling region, the two temperature peaks occur in early June and the middle of September, respectively. The 5m-depth temperature comes to an annual minimum in early February, rising from March, and then reaches the first peak in the early June. Theoretically, while entering summer, the sea surface net heat flux increases as the solar radiation is enhanced and the SST should monotonously rise. However, the modeled subsurface temperature decreases continuously rather than increases, and reaches the summer's lowest point at the middle of July, and then rises gradually to the second peak at the middle of September. The subsurface temperature

variation in the YD is similar to that in the QD, but the two peaks of temperature time series lie in the middle of July and early September. The summer's lowest temperature at 5m-depth occurs in the middle of the August, which is about one month later than that in the QD. These modeled results suggest that there must be other factors cooling the seawater in the QD and YD upwelling regions and affecting their seasonal temperature variations besides the solar radiation. In summer, there is no cold water source at the same horizontal level around the QD and YD upwelling regions, so it is clear that the cold pools in the QD and YD are closely related to the deep water upwelling.

From the above analysis, we can find that there clearly are summer upwellings in the NCSCS. The typical continental shelf upwelling characteristics are revealed at the surface and subsurface in the two strong upwelling regions, QD and YD. And the modeled temperature at 5m-depth shows the seasonal variation of the typical "two-peak distribution". It also suggests the summer upwelling is a seasonal phenomenon during June-September in the NCSCS.

5. Discussion

5.1 Relationship between the upwelling and local winds

The summer upwelling in the NCSCS is a very complicated hydrokinetic process, which is affected by many factors including the bottom topography, summer southwest winds, shelf currents, eddies, air-sea flux, islands and capes, etc. Knowledge of its dynamic mechanisms is limited. The local wind has been confirmed as one of the most important dynamical factors to drive the NCSCS upwelling in previous literatures (Wyrtki, 1961; Li, 1990; Hong and Li, 1991; Zhuang et al., 2005). In this study, the QuikSCAT scatterometer wind data are analyzed, and the impacts of coastal winds on to the coastal upwelling are further investigated, including the alongshore wind stress and local

wind stress curl.

The wind stress curl is defined as $Curl_z = \frac{\partial(\tau_y)}{\partial x} - \frac{\partial(\tau_x)}{\partial y}$ (6)

and the vertical velocity caused by Ekman pumping is defined as

$$\omega_e = \left[\frac{\partial(\tau_y)}{\partial x} - \frac{\partial(\tau_x)}{\partial y}\right] \Big/ \rho_0 f = Curl_z \Big/ \rho_0 f \quad (7)$$

Here τ_x and τ_y represent the meridional and zonal wind stress respectively; and ρ_0 is the density of seawater, 1.025×10^3 kg/m^3; f is the coriolis parameter. The climatological distribution of wind stress curl in summer upwelling season is shown in Figure 9, which is calculated with equations (6) in the Cartesian coordinate system. The vertical velocity caused by Ekman pumping can be obtained with equation (7). It is obvious that the climatological wind stress curl in summer upwelling season is positive in the whole eastern coast of the Hainan Island, where the mean wind stress curl is 0.27×10^{-6} N/m^3 and the upwelling velocity caused by wind stress curl is about 0.7×10^{-5} m/s, which is considerable. At the same time, the position of strong Ekman pumping is coincided with that of the modeled strong upwelling in the QD, which suggests that the wind stress curl has a very important and active contribution to the QDU.

On the other hand, the stable southwest monsoon during summer can drive the offshore Ekman transport, which can directly result in the deep nutrient-rich water upwelling to the upper layer. The correlation coefficients between the modeled SST at 5m-depth and the wind stress curl and the alongshore wind stress in the QD are 0.694 and 0.572 respectively (Figure 8 (a)). It indicates that both the alongshore wind stress-driven Ekman transport and the wind stress curl-induced Ekman pumping have very important and favorable contributions to forming the coastal upwelling in the QD. But in the YD the mechanism is different from that of the QD. As shown in Figure 9, the wind

stress curl in the YD is small everywhere, no more than 0.05×10^{-6} N/m^3 and even negative in some places. This indicates that the local wind stress curl in the YD has little active contribution or even unfavorable to the YDU. But with the effects of Coriolis force and geostrophic balance, the southwest alongshore wind stress drives the seawater of upper layer moving offshore. Therefore, the deeper water has to upwell to compensate the upper lost water, which can directly induce the coastal upwelling. At the same time, modeled results show the high correlation between the modeled SST at 5m-depth and the alongshore wind stress, with the correlation coefficient of 0.637 (Figure 8 (b)), which suggests the alongshore wind stress-driven Ekman transport has an important and favorable contribution to the YDU even though the summer local wind stress curl has negligible or unfavorable effect on the YDU.

5.2 Effects of wind stress and wind stress curl on the Upwelling

Four numerical experiments (Table 2) are designed for better understanding the effects of the wind stress and wind stress curl on the NCSCS upwelling. Figure 10-12 shows the vertical profiles of the standard deviation of modeled temperature, salinity and potential density of each case. In Section I (Figure 10), with no wind forcing (Case A) the coastal upwelling is weak with the VPDG of 1.63×10^{-4} and the upwelling mainly occurs in the subsurface layer deeper than 20m. In Case B, the model is forced by the spatial uniform southwest wind 8 m/s but without wind stress curl. The coastal upwelling is enhanced remarkably, and the colder nutrient-richer water at the depth shallower than 50m is uplifted to the surface with the seaward extent of 100 km. The VPDG is 4.11×10^{-4}, about 2.5 times of Case A, which reflects the significant effect of wind stress on the YDU. While the QuikSCAT wind stress curl is considered in Case C, the upwelling intensity of

Section I is not increased compared with that in Case B, instead, the VPDG has decreased to 3.78×10^{-4}. In Case D, when the model is forced by the double wind stress and wind stress curl of Case C, the upwelling is strongly enhanced and the VPDG reaches 5.39×10^{-4}, about 1.5 times of Case C. So it can be found from the numerical experiments that the local wind has a significant effect on the YDU. The dominant alongshore wind stress-driven Ekman transport has a significant contribution to the coastal upwelling but the wind stress curl is little active and even unfavorable to the YDU.

The upwelling response to the local winds in the QD is different from that in YD. Shown in the Figure 11, in Section II with no wind forcing (Case A), the upwelling still occurs but the intensity is abnormally small with the VPDG of only 1.41×10^{-4}. While the alongshore wind stress is included and wind stress curl is still excluded (Case B) the coastal upwelling is vivid with the VPDG of 2.43×10^{-4}, which is 70% stronger than that of Case A. In Case C, the QuikSCAT wind stress and wind stress curl are all considered, both of isotherm and isohaline over the shelf are all uplifted towards the shore significantly and VPDG reaches 4.37×10^{-4}, about 3 times that of Case A and 80% stronger than that of Case B. Similarly in Case D, the QuikSCAT wind forcing is doubled to that of Case C. The results show that the averaged gradients of isotherm and isohaline are further enhanced and the APDG reaches 8.03×10^{-4}. Compared with the results of Section I, not only the offshore Ekman transport driven by the alongshore wind stress, the wind stress curl-induced Ekman pumping is also an important contribution to cause the coastal upwelling along Section II. The upwelling index VPDG also indicate that the wind stress curl is a more important dynamic factor than the alongshore wind stress in inducing the coastal upwelling.

The Section III is located in the continental shelf break of southern Lingshui Bay. Figure 12

shows both isotherm and the isohaline are uplifted to the onshore direction in above four cases, and the VPDG of each of cases is 4.73×10^{-4}, 5.71×10^{-4}, 9.00×10^{-4} and 1.25×10^{-3}, respectively. It can be found that in Section III not only alongshore wind stress but also wind stress curl play important roles in forming the coastal upwelling in summer. On the other hand, it is noted that the VPDG of Case B is 21% more than that of Case A and the APDG of Case C is 58% more than that of Case B, which indicates that the wind stress curl has a more important effect to induce the coastal upwelling in Section III, which is applied to Section II as well. Therefore, the analysis of experimental results in Section II and III of the QD shows that the local winds play crucial roles in causing the coastal upwelling and the wind stress curl is more important than the alongshore wind stress to induce the QDU.

6. Summary and Conclusion

In present study, the summer upwelling in the NCSCS is successfully simulated by a three-dimensional baroclinic nonlinear prognostic numerical model forced by the QuikSCAT winds. By combining climatological AVHRR SST image, field observations and numerical simulation, the summer upwelling in the NCSCS is confirmed as a seasonal common phenomenon during June-September with the spatial extent of a basin-scale in the NCSCS. Furthermore, an improved understanding on the NCSCS upwelling system and the different dynamics mechanism of wind stress curl inducing the coastal upwelling in the QD and YD are obtained. The conclusions of this study are as follows.

(1) The summer upwelling is a seasonal common phenomenon during June-September with the spatial extent of a basin-scale in the NCSCS. The typical continental shelf upwelling

characteristics are clearly shown in the surface and subsurface water of upwelling regions, such as low temperature, high salinity and high density.

(2) There are two large and strong upwelling regions in the NCSCS, one of them is located in the east of the Hainan Island, the east of the Leizhou Peninsula and the southeast of the Zhanjiang Bay, and the other one is located in the inshore area from the Shantou Coast to the Nanri Islands.

(3) The upwelling centres of QDU are located at (111°10′E, 19°45′N) between the Qinglan Bay and the Qizhou Archipelagoes and (110°15′E, 18°25′N) near the Lingshui Bay; and those of YDU are mainly located at (116°45′E, 22°50′N) and (118°E, 23°40′N) near the Shantou Coast and the Taiwan Shoal.

(4) The local winds, as the important dynamic factors, have crucial roles to cause the coastal upwellings in both of QD and YD. In the QD, the alongshore wind stress and local wind stress curl all have significant and favorable contributions to cause the summer coastal upwelling, and the correlation coefficients, between the upwelling index and local wind stress curl, and the upwelling index and alongshore wind stress, are 0.694 and 0.572 respectively. However, in the YD, only the alongshore wind stress is the dominant dynamic factor to drive the coastal upwelling, with the correlation coefficients between the upwelling index and alongshore wind stress of 0.637, and the contribution of local wind stress curl is negligible and even unfavorable to the YDU.

It is well-known that the upwelling has a significant effect on fisheries and coastal environmental protection in the NCSCS. The upwelling system in the NCSCS is very complicated, and the understanding of it is limited. For the last decade, satellite remote sensing technology has

been revolutionizing ocean observation, enabling us to make routine and high-resolution measurements of SST, sea surface height (SSH), ocean color, and surface winds over the world ocean. Taking advantage of these new technologies, the investigations on the interannual variations of the coastal upwelling, the relationship with ENSO and regional climate change will be carried out in the future. At the same time, the field observations of ocean and atmosphere have also been proposed in the coastal upwelling regions for further studying the coastal jet, cold filaments, coastal eutrophication and their dynamical mechanisms in the NCSCS upwelling system.

7. Acknowledgements

The survey observational data are derived from the '908' Special Marine Survey during 2006 summer. The AVHRR SST data is obtained from JPL of NASA. The products of QuikSCAT winds data were produced by the IFREMER at the Department of Oceanography from Space (LOS+CERSAT), and the WOA01 temperature and salinity are distributed by the Ocean Climate Laboratory (OCL) of National Oceanographic Data Centre (NODC) and the heat flux data were provided by the National Oceanography Centre, Southampton (NOCS). This research is supported by grants from the Chinese Academy of Sciences (Grant No: kzcx2-yw-201), the National Basic Research Program of China (No: 2006CB403604). Supports are also provided by the State Key Laboratory Science Foundation (No: 2005406811), National Natural Science Foundation of China (No: 50679019 and No. 50009001), Social Science and Technology Development Project of Jiangsu Province (No: BS2006095) and 908 Special Foundation of Jiangsu Province (No: JS-908-02-06).

References

Josey, S.A., 2001. A Comparison of ECMWF, NCEP-NCAR and SOC Surface Heat Fluxes with Moored Buoy Measurements in the Subduction Region of the Northeast Atlantic. Journal of Climate 14(8), 1780-1789.

Blumberg, A.F., 1996. An Estuarine and Coast Ocean Version of POM. Proceedings of the Princeton Ocean Model Users Meeting, Princeton, N. J.

Boyer, T.P., Stephens, C., Antonov, J.I., Conkright, M.E., Locarnini, R.A., O'Brien, T.D., Garcia, H.E., 2002. In: Levitus, S. (Ed.), World Ocean Atlas 2001, Volume 1: Salinity. NOAA Atlas NESDIS 50, US Government Printing Office, Washington DC, 176-182.

Blanke, B., Speich, S., Bentamy, A., Roy, C., Saw, B., 2005. Modeling the structure and variability of the southern Benguela upwelling using QuickSCAT wind forcing. Journal of Geophysical Research 110, 1-18.

Cai, W.J., Lennon, G.W., 1988. Upwelling in the Taiwan Strait in Response to Wind Stress, Ocean Circulation and Topography. Estuarine, Coastal and Shelf Science 26, 15-31.

Chen, J.Q., Fu, Z.L., Li, F.X., 1982. A Study of Upwelling over Minnan-Taiwan Shoal Fishing Ground. Journal of Oceanography in Taiwan Strait 1(2), 5-13. (in Chinese)

Fang, G.H., Zhao, B.R., Zhu, Y.H., 1991. Water Volume Transport through the Taiwan Strait and the Continental Shelf of the East China Sea Measured with Current Meters. In: Takano, K. (Eds.), Oceanography of Asian Marginal Seas. Elsevier, Amsterdam, 345-358.

Guan, B.X., Cheng, S.J., 1964. Ocean Current system in East China Sea and South China Sea. Qingdao, Institute of Oceanology, Chinese Academy of Sciences. (in Chinese)

Guo, F., Si, M.C., Xia, Z.W., 1998. Two-dimension diagnose model to calculate upwelling on offshore of the east coast of Hainan Island. Acta Oceanologica Sinica 20, 109-116. (in Chinese)

Han, W.Y., Ma, K.M., 1988. Study of Yuedong Coastal Upwelling. Acta Oceanologica Sinica 10, 52-59.

Han, W.Y., Wang, M.B., Ma, K.B., 1990. The lowest surface water temperature area of China Sea in summer - the upwelling along the east coast of Hainan Island. Oceanologia Et Limnologia Sinica 21, 167-275. (in Chinese)

Hong, H.S., Qiu, S.Y., Ruan, W.Q., Hong, Q.C., 1991. Minnan-Taiwan Bank fishing ground upwelling ecosystem study. In Hong, H.S., Qiu, S.Y., Ruan, W.Q., Hong, Q.C. (Eds.), Minnan-Taiwan Bank fishing ground upwelling ecosystem study. Beijing, China: Science Publishing House. (in Chinese)

Hong, Q.M., Li, L., 1991. A study of upwelling over continental shelf off eastern Guangdong. Journal of Oceanography in Taiwan Strait 10(3), 272-277. (in Chinese)

Hu, J.Y., Kawamura, H., Hong, H.S., Pan, W.R., 2003. A Review of Research on the Upwelling in the Taiwan Strait. Bulletin of Marine Science 73(3), 605-628.

Hu, J.Y., Kawamura, H., Hong, H.S., Suetsugu, M., Lin, M.S., 2001. Hydrographic and Satellite Observations of Summertime Upwelling in the Taiwan Strait: A Preliminary Description. Terrestrial, Atmospheric and Oceanic Sciences 12(2), 415-430.

Jing, Z.Y., Hua, Z.L., Qi, Y.Q., Zhang, H., 2007. Summer upwelling in the northern continental shelf of the South China Sea, Proceedings of the 16th Australasian Fluid Mechanics Conference. School of Engineering, the University of Queensland, Queensland, Australia, 782-785.

Li, L., 1990. A study on the summer upwellings in shelf waters west to Zhujiang River mouth. Journal of Oceanography in Taiwan Strait 4, 338-346. (in Chinese)

Li, L., 1993. Summer upwelling system over the northern continental shelf of the South China Sea-physical description. Proceedings of the Symposium on the Physical and Chemical Oceanography of the China Seas. Beijing: China Ocean Press, 58-68. (in Chinese)

Li, L., Li, D., 1989. Summer Hydrographic features of Channel West of Taiwan Shoals and the Coastal Upwelling. Journal of Oceanography in Taiwan Strait 8(4), 353-359. (in Chinese)

Mellor, G.L., Yamada, T., 1982. Development of a Turbulence Closure Mode Geophysical Fluid Problems, Reviews of Geophysics and Space Physics 20, 851-875.

Niino, H., Emery, O., 1961 Sediment of shallow portions of East China Sea and South China Sea, Geological Society of American Bulletin 72, 731-761.

Pauly, D., Christensen, V., 1995. Primary production required to sustain global fisheries. Nature 374, 255-257.

Risien, C.M., Mellor C.J., Reason, C., Shillington, F.A., Chelton, D.B., 2004. Variability in satellite winds over the Benguela upwelling system during 1999-2000. Journal of Geophysical Research 109, 1-15.

Shang, S.L., Zhang, C.Y., Hong, H.S., Shang, S.P., Chai, F., 2004. Short-term Variability of Chlorophyll Associated with Upwelling Events in the Taiwan Strait during the Southwest Monsoon of 1998. Deep-Sea Research II 51, 1113-1127.

Smagorinsky, J., 1963. General Circulation Experiments with the Primitive Equations, I. The Basic Experiment. Monthly Weather Review 91, 99-164.

Su, J.L., 2004. Overview of the South China Sea circulation and its influence on the coastal physical oceanography outside the Pearl River Estuary. Continental Shelf Research 24, 1745-1760.

Tang, D.L., Kester, D.R., Ni, I.H., Kawamura, H., Hong, H.S., 2002. Upwelling in the Taiwan Strait during the summer monsoon detected by satellite and shipboard measurements, Remote Sensing of Environment 83, 457-471.

Tang, D.L., Kawamura, H., Guan, L., 2004, Long-time observation of annual variation of Taiwan Strait Upwelling in Summer Season, Advances in Space Research 33, 307-312.

Wu, R.S., Li, L., 2003. Summarization of study on upwelling system in the South China Sea, Journal of Oceanography in Taiwan Strait 22, 269-277. (in Chinese)

Wyrtki, K., 1961. Physical oceanography of the Southeast Asia waters, NAGA Report 2, 1-195.

Xiao, H., 1988. Studies of Coastal Upwelling in Western Taiwan Strait. Journal of Oceanography in Taiwan Strait 7(2), 135-142. (in Chinese)

Yan, Z.T., Li, H.Y., Yu, G.Y., 1997. Numerical Study on the Upwelling along the Fujian Coast. Journal of Oceanography in Taiwan Strait 19(5), 13-19. (in Chinese)

Yu, W.Q., 1987. A preliminary approach of the upwelling for the northern South China Sea. Marine Science 6, 7-10.

Zeng, L.M., 1986. A preliminary analysis of indicators of offshore upwelling off eastern Guangdong. Journal of Tropic Oceanology 5, 68-73. (in Chinese)

Zhuang, W., Wang, D.X., Wu, R.S., Hu, J.Y., 2005. Coastal Upwelling off Eastern Fujian-Guangdong Detected by remote Sensing, Chinese Journal of Atmospheric Sciences 29, 438-444.

Figure Captions

Figure 1. (a) Bathymetry (unit: m) of the South China Sea (The domain within in the red rectangle is the study area). The four lateral boundaries A-D are specified with the blue dot lines. (b) Map of the study domain, the NCSCS. SA - Shanya; LSB - Lingshui Bay; QLB - Qinglan Bay; QZA - Qizhou Archipelagoes; ZJB - Zhanjiang Bay; LP - Leizhou Peninsula; GC - Guangdong Coast; FC - Fujian Coast; SFC - the South of Fujian Coast; ST - Shantou; XM - Xiamen; NRI - Nanri Islands; TWS - Taiwan Shoal. Three typical cross-shelf sections are indicated in blue lines.

Figure 2. Climatological summer SST derived from the AVHRR in the NCSCS (unit:℃). QDU - the Upwelling in the Qiongdong; YDU - the Upwelling in the Yuedong.

Figure 3. Map of survey route and stations. The survey was conducted during 19 July to 06 August 2006 in the east of the Hainan Island, which included 13 cross-shelf sections (D01-D13). Red lines and dots represent the cruise route and stations, respectively. The black lines show the isobaths in meters.

Figure 4. Horizontal distributions of the observed temperature and salinity in the depth of 10m, 20m, 30m and 50m, respectively. The field survey was performed during19 July to 06 August 2006.

Figure 5. Vertical distributions of the observed temperature and salinity in the typical section D02, D03, D08 and D09, respectively. The field survey was performed during 19 July to 06 August 2006.

Figure 6. Horizontal distributions of modeled current vectors in the South China Sea (SCS) at depths of 5m layer.

Figure 7. Modeled results of temperature and salinity in the northern continental shelf of the South China Sea (NCSCS). a. Temperature at 5m-depth; b. Temperature at 15m-depth; c. Salinity at 15m-depth; d. Potential density at 15m-depth.

Figure 8. Time series of the temperature at 5m-depth, QuikSCAT alongshore wind stress, and wind stress curl averaged in the two typical strong upwelling regions, QDU and YDU. a. Time series in the QDU; b. Time series in the YDU.

Figure 9. The horizontal distribution of climatological summer wind stress curl in the northern continental shelf of the South China Sea (NCSCS) (unit: 10^{-6} N/m^3).

Figure 10. Numerical experiment results in Case A, B, C and D: vertical distributions of modeled temperature, salinity and potential density standard deviations in Section I. Section I is located in the south of Fujian Coast.

Figure 11. Numerical experiment results in Case A, B, C and D: vertical distributions of modeled temperature, salinity and potential density standard deviations in Section II. Section II is located near the Qinglan Bay.

Figure 12. Numerical experiment results in Case A, B, C and D: vertical distributions of modeled temperature, salinity and potential density standard deviations in Section III. Section III is located in the south of Lingshui Bay.

Table Captions

Table 1. Monthly throughflows through lateral boundaries (unit: 10^6 m^3/s).

Table 2. Numerical Experiment Schemes

1 Table 1. Monthly throughflows through lateral boundaries (unit: 10^6 m^3/s).

Month	Lateral Boundaries			
	A	B	C	D
January	-3.125	27.375	-23.625	-0.625
February	-2.250	29.000	-26.000	-0.750
March	-0.750	31.000	-29.000	-1.250
April	0.750	32.375	-31.500	-1.625
May	2.250	33.125	-33.500	-1.875
June	3.000	32.625	-33.500	-2.125
July	3.000	30.875	-31.500	-2.375
August	2.125	29.875	-29.625	-2.375
September	0.375	29.625	-27.875	-2.125
October	-1.250	28.500	-25.500	-1.750
November	-2.750	26.500	-22.500	-1.250
December	-3.375	26.125	-21.875	-0.875

2

3

Table 2. Numerical Experiment Schemes[a]

	Wind Stress	Wind Stress Curl
Case A	N	N
Case B	Y	N
Case C	Y	Y
Case D	D	D

[a]‘ Y’ means that the effect is considered in the model, ‘N’ means that the effect is excluded from the model, and the ‘D’ means that the effect is doubled in the model.

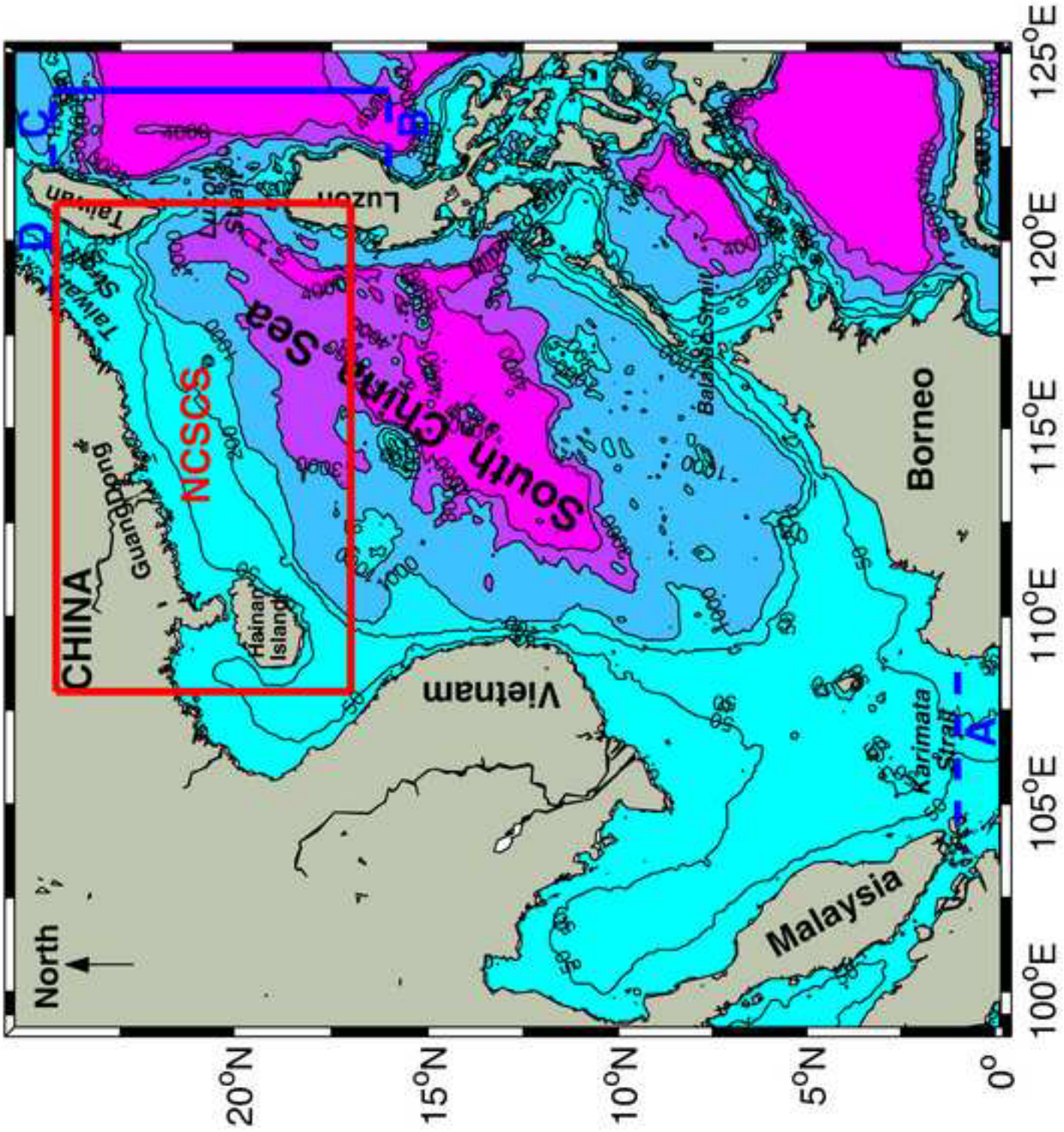
D
C
B
A
NCSCS
South China Sea
CHINA
Guangdong
Hainan Island
Taiwan Strait
Luzon
Balabac Strait
Borneo
Vietnam
Karimata Strait
Malaysia
North
100°E
105°E
110°E
115°E
120°E
125°E
0°
5°N
10°N
15°N
20°N

Figure 1 (a)

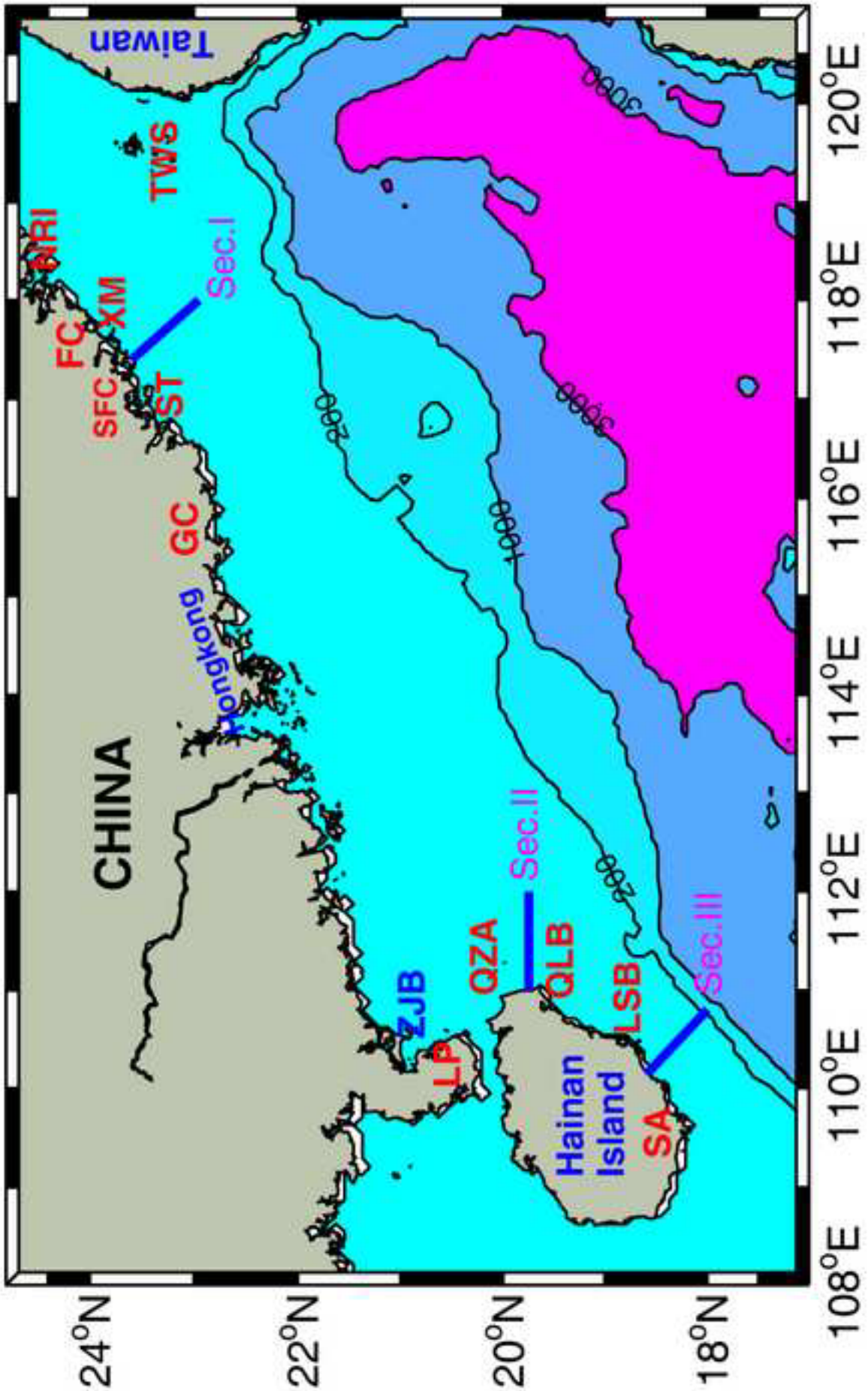
Taiwan
TWS
NRI
FC
XM
SFC
ST
Sec.I
GC
Hongkong
CHINA
200
1000
3000
5000
ZJB
LP
QZA
Sec.II
QLB
LSB
Sec.III
Hainan
Island
SA
24°N
22°N
20°N
18°N
108°E
110°E
112°E
114°E
116°E
118°E
120°E

Figure 1 (b)

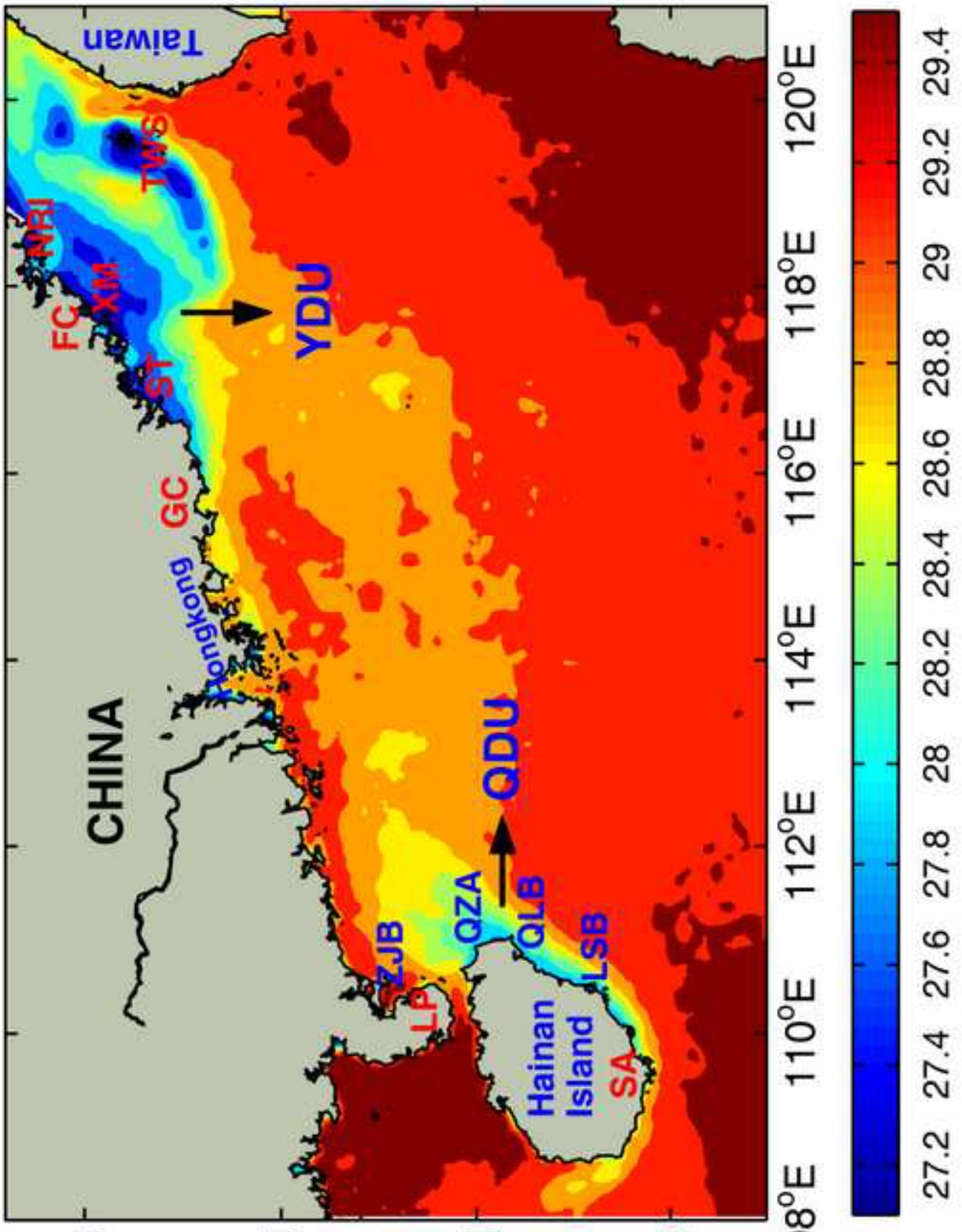
Taiwan
CHINA
Hongkong
Hainan
Island
FC
NRI
XMI
TWS
ST
GC
YDU
QDU
ZJB
LP
QZA
QLB
LSB
SA
24°N
22°N
20°N
18°N
108°E
110°E
112°E
114°E
116°E
118°E
120°E
27.2
27.4
27.6
27.8
28
28.2
28.4
28.6
28.8
29
29.2
29.4

Figure 2

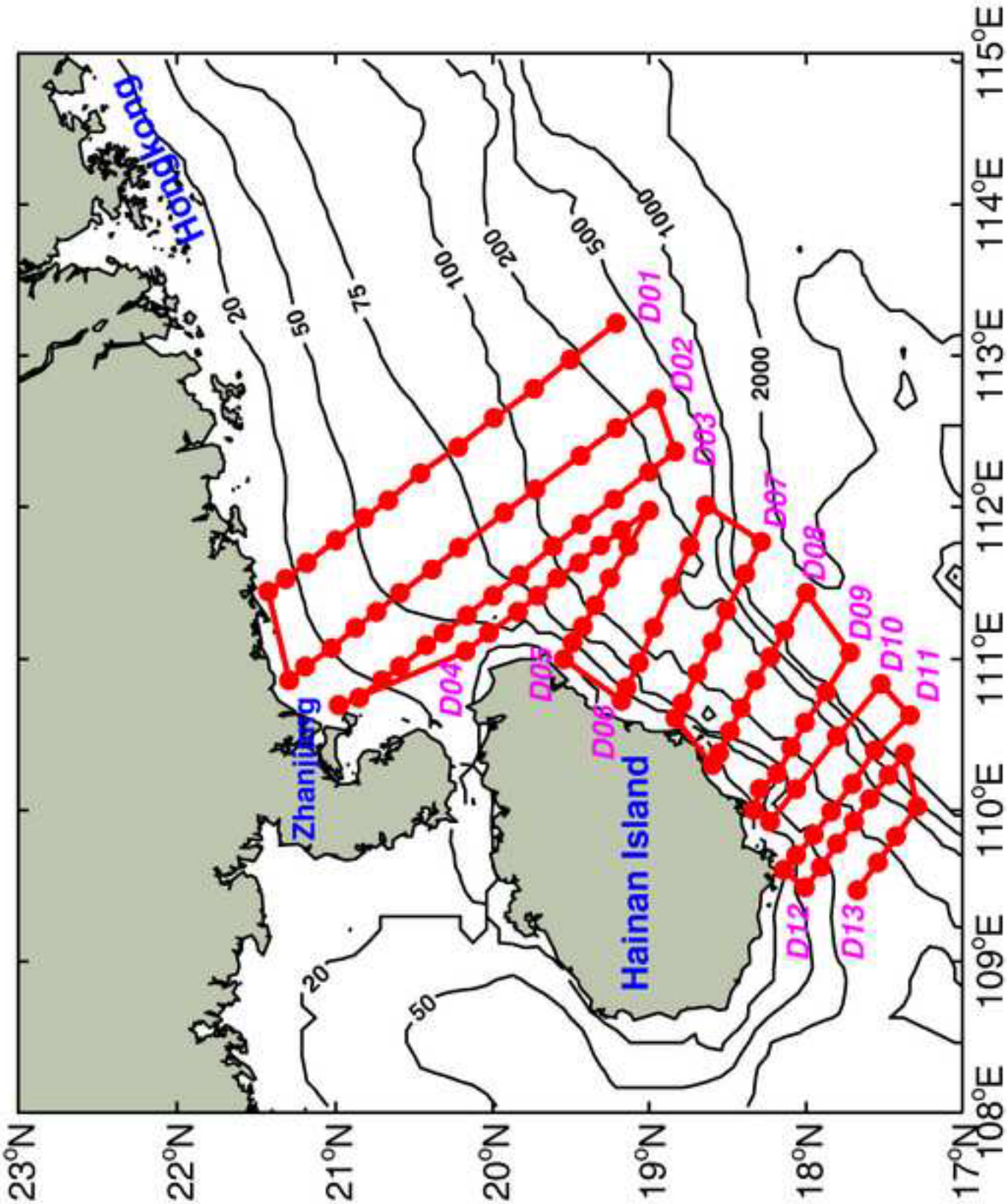
Hong Kong
Zhanjiang
Hainan Island
D01
D02
D03
D04
D05
D06
D07
D08
D09
D10
D11
D12
D13
20
50
75
100
200
500
1000
2000
23°N
22°N
21°N
20°N
19°N
18°N
17°N
108°E
109°E
110°E
111°E
112°E
113°E
114°E
115°E

Figure 3

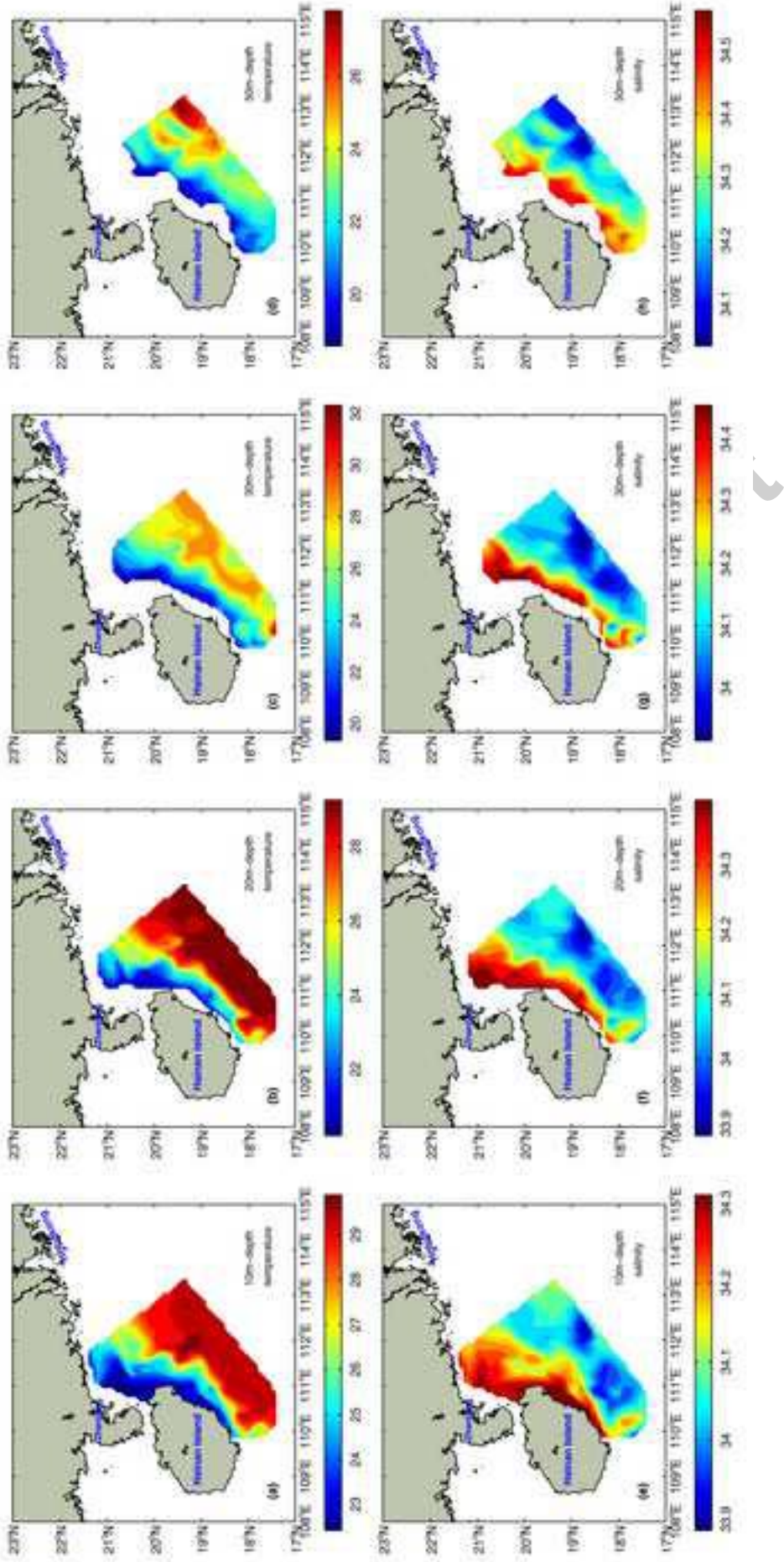

Figure 4

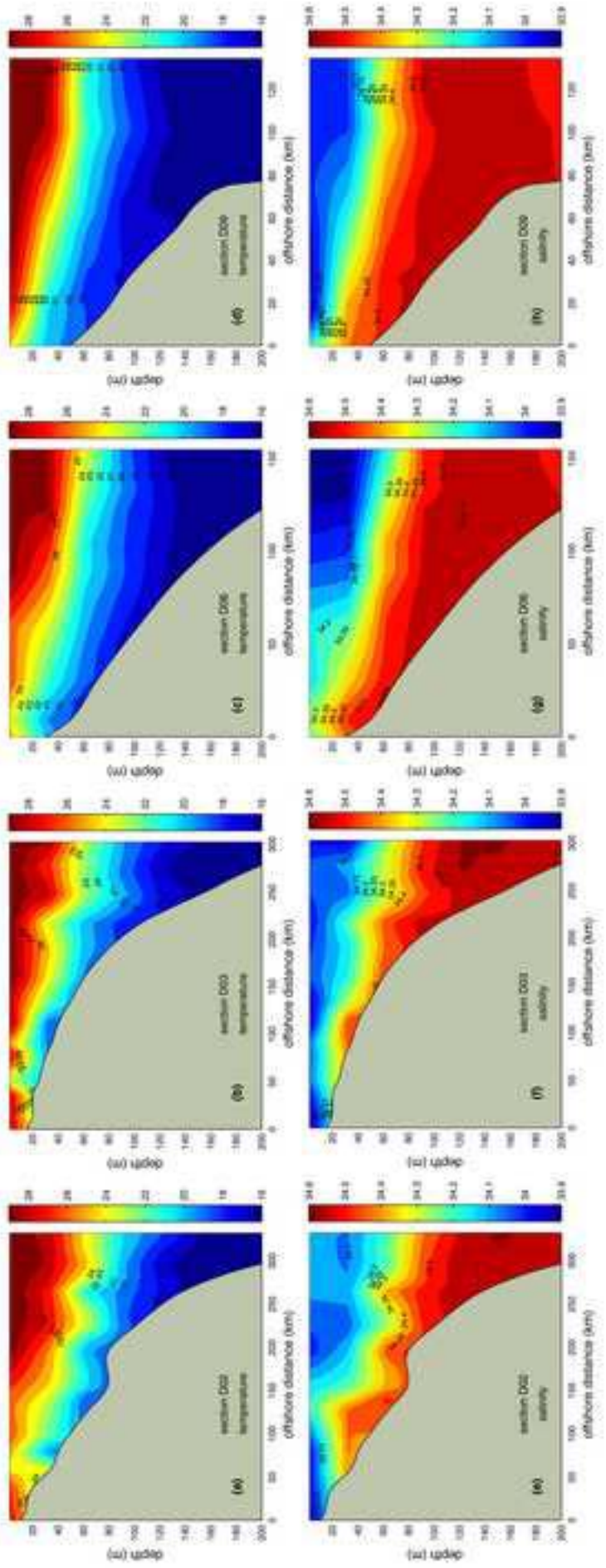
section D09
temperature
(h)
section D09
salinity
(g)
section D06
temperature
(e)
section D06
salinity
(d)
section D03
temperature
(b)
section D03
salinity
(f)
section D02
temperature
(a)
section D02
salinity
(c)
offshore distance (km)
depth (m)

Figure 5

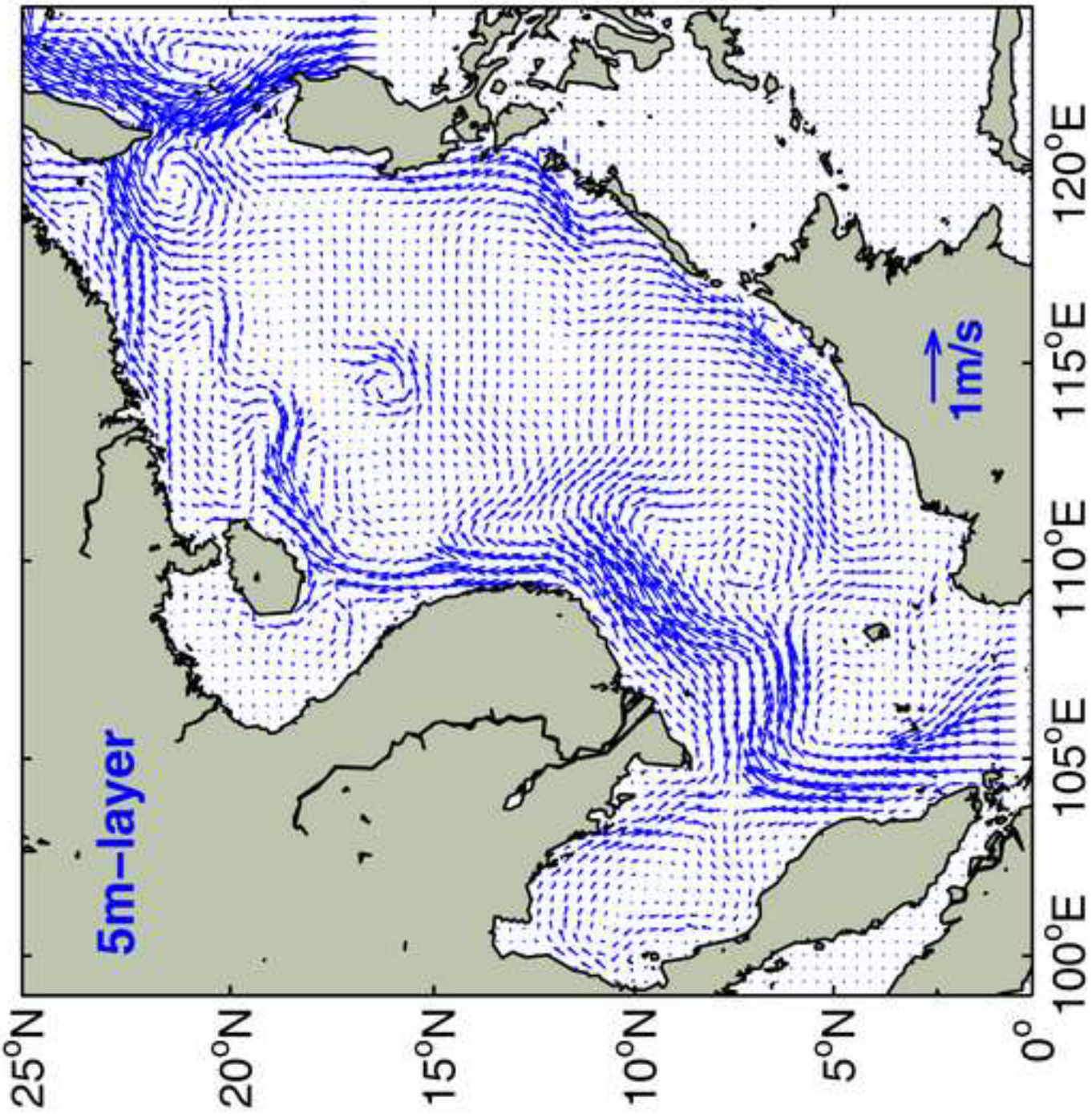

Figure 6

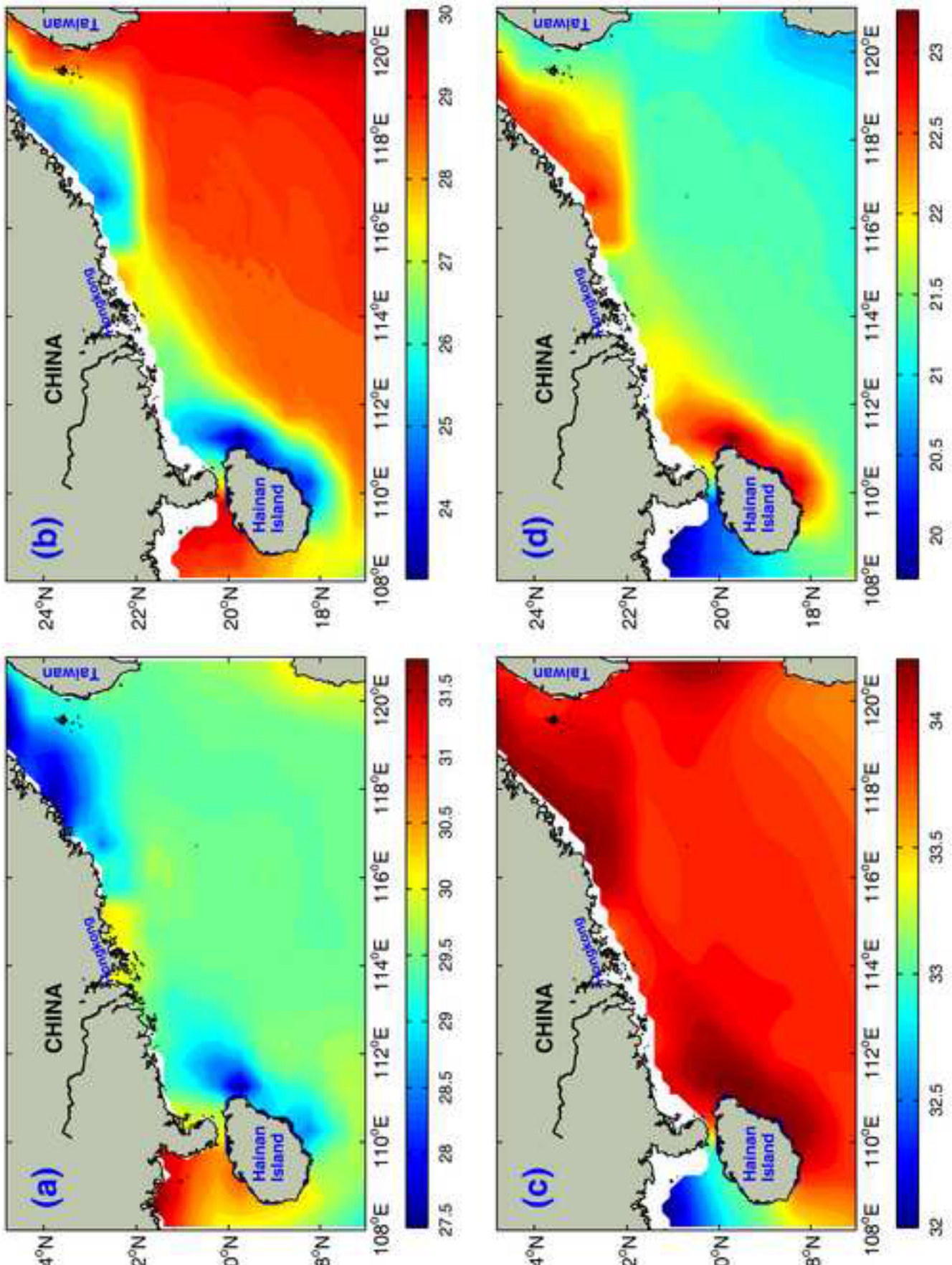

Figure 7

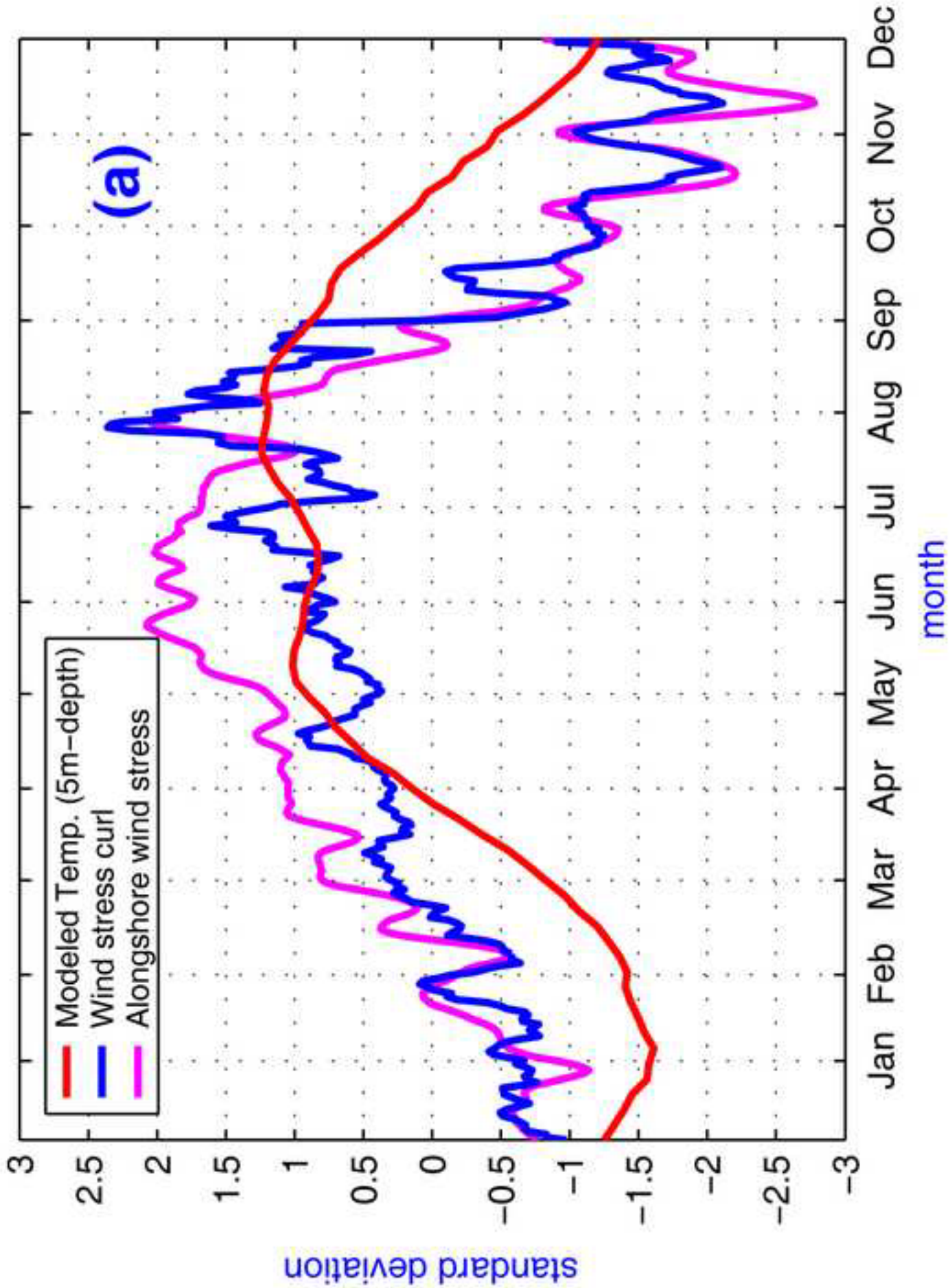

Figure 8 (a)

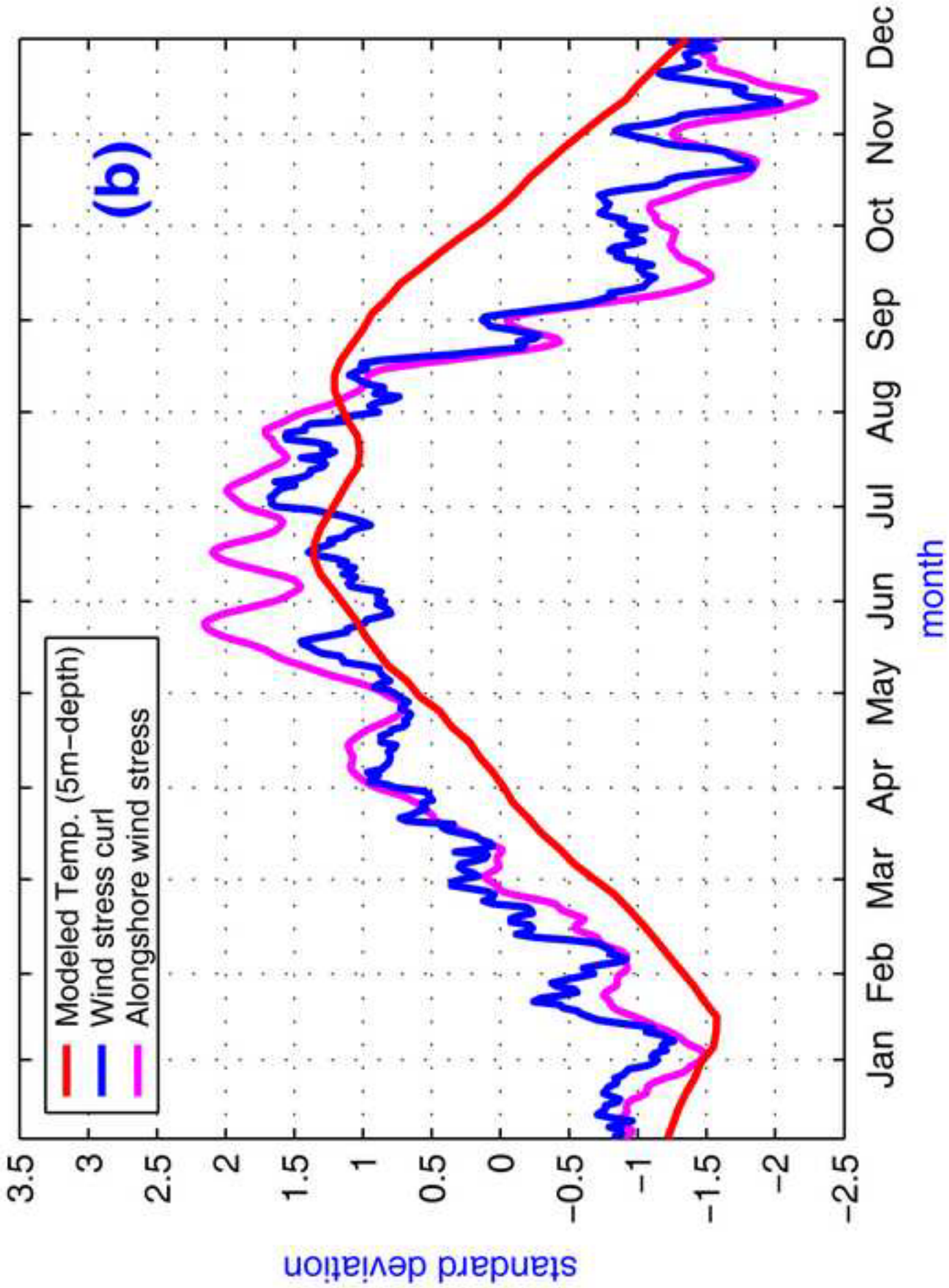

Figure 8 (b)

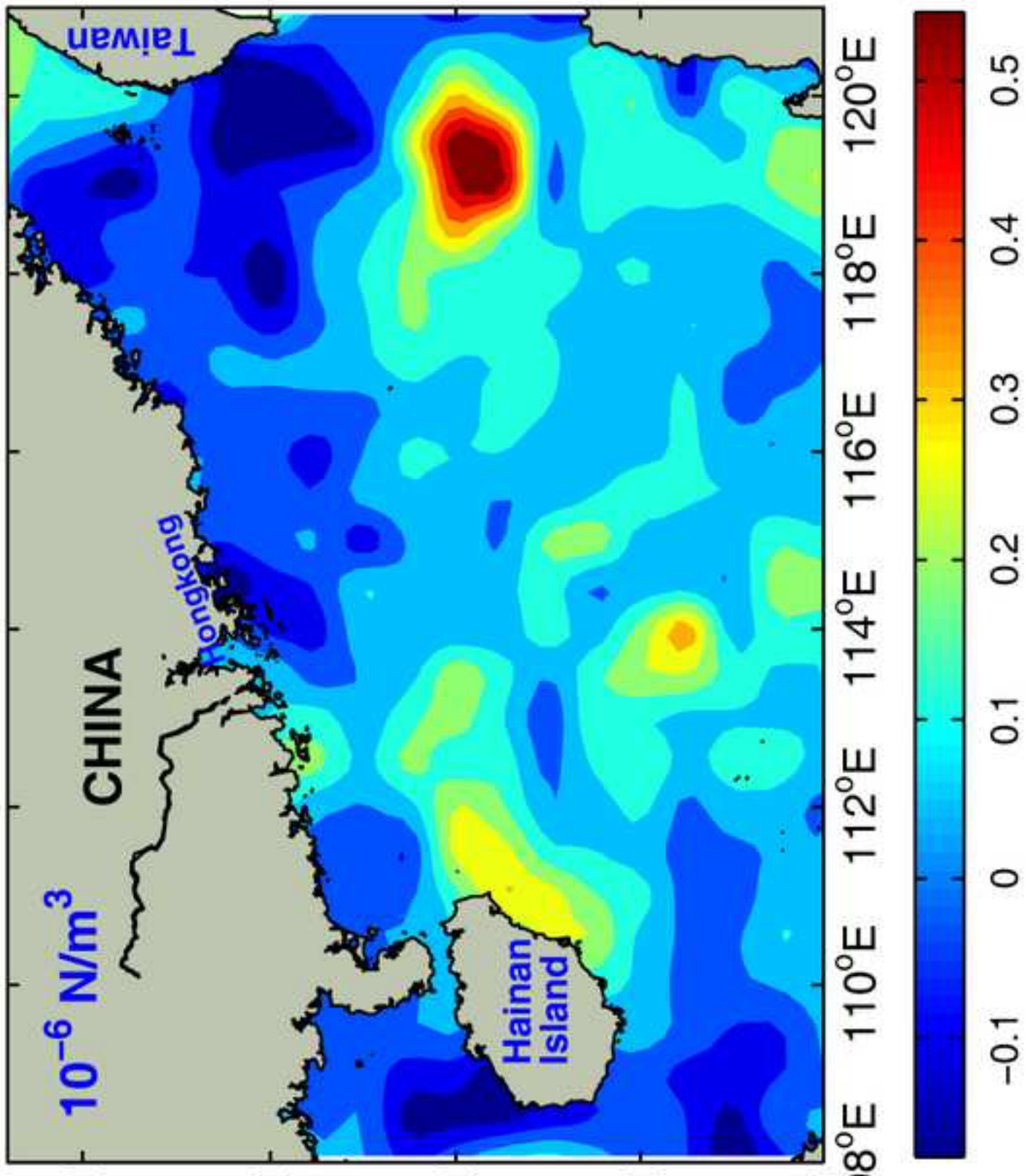
Taiwan
CHINA
Hongkong
Hainan Island
10^{-6} N/m^3
24°N
22°N
20°N
18°N
16°N
108°E
110°E
112°E
114°E
116°E
118°E
120°E
−0.1
0
0.1
0.2
0.3
0.4
0.5

Figure 9

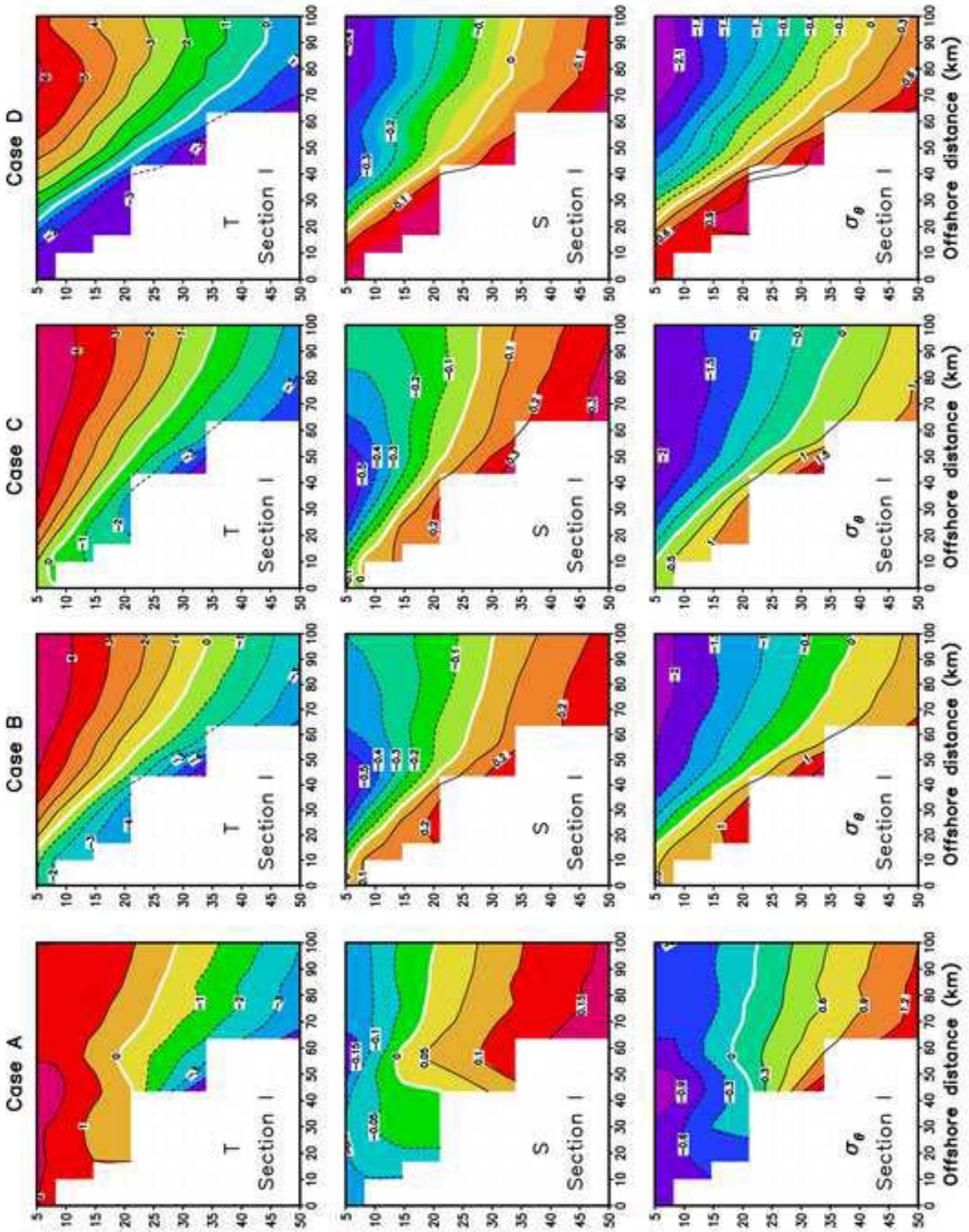
Case A
Case B
Case C
Case D
T
S
σ_θ
Section I
Depth (m)
Offshore distance (km)

Figure 10

Figure 11

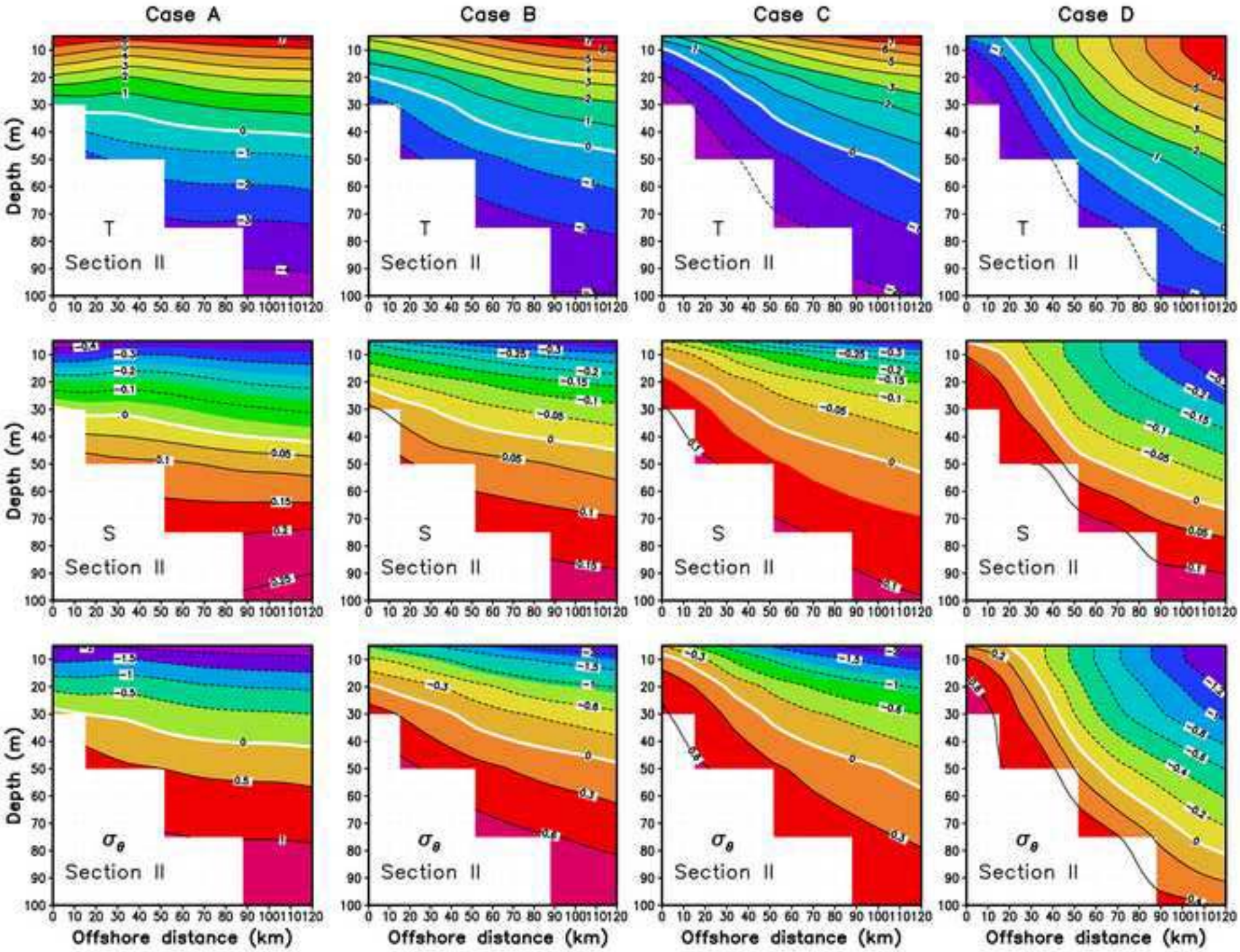

Figure 12